

Received July 25, 2020, accepted August 11, 2020, date of publication August 14, 2020, date of current version August 26, 2020.

Digital Object Identifier 10.1109/ACCESS.2020.3016895

Transient Electromagnetic Voltage Imaging of Dense UXO-Like Targets Based on Improved Mathematical Morphology

XUEGUI ZHU^{1,2}, YU SHU¹, CHAOPENG LUO², FUSHUO HUO¹, AND WANG ZHU³

¹State Key Laboratory of Power Transmission Equipment and System Security and New Technology, Chongqing University, Chongqing 400044, China

²Science and Technology on Near-Surface Detection Laboratory, Wuxi 214035, China

³School of Microelectronics and Communication Engineering, Chongqing University, Chongqing 400044, China

Corresponding author: Xuegui Zhu (zhuxuegui@cqu.edu.cn)

This work was supported by the Fund of Science and Technology on Near-Surface Detection Laboratory of China under Grant 614241409041417.


ABSTRACT Unexploded ordnance (UXO) survey is the foremost task of clearance project. Transient electromagnetic method (TEM) is proved effective for UXO survey. However, it is still difficult for TEM to detect small-size, ultra-shallow and dense UXO targets because the large-size devices and inversion methods for large-scale applications are usually ineffective. In the work, in order to avoid the complex inversion of apparent resistivity, the voltages acquired by our specified small-loop TEM system are used to depict a voltage distribution profile, which is then processed with an improved imaging algorithm. Several major influences on the secondary voltage image are discussed during UXO survey, including emitting coil size, target attitude, basin effect and shell thickness. Furthermore, an improved watershed imaging algorithm is proposed to obtain the best threshold marking and automatically realize the dense target discrimination. Over-segmentation resulting from burrs, noises, and scraps is reduced through background marking. And also under-segmentation is avoided during foreground marking through adaptive search of saddle point. The algorithm has been verified effective using simulation data and experiment data of UXO-like targets.

INDEX TERMS Transient electromagnetic method, unexploded ordnance, image segmentation, watershed transform, adaptive saddle point search.

I. INTRODUCTION

It is reported that there are about one hundred million pieces of unexploded ordnance (UXO) distributed in more than 100 countries, which are endangering our environment, engineering construction and human safety [1]. UXO survey is the foremost task in clearance project of UXO and one of the popular research topic all over the world. However, the UXO targets are distributed scatteredly, have small sizes and located 0.3m to 8m underground with serious human interference. So it is very difficult to find the UXO when compared with the big and deep targets, such as metal minerals and bunkers underground.

The main survey methods for UXO include magnetic survey [2]–[4], electromagnetic method [5], [6] and ground penetrating radar (GPR) [7]. The magnetic survey is widely used

The associate editor coordinating the review of this manuscript and approving it for publication was Abdel-Hamid Soliman .

to find UXO when the survey devices are mounted on the ground, in the water or the air. However, the magnetic survey is not suitable for the non-magnetic targets and behaves badly with a high false alarm rate if there are lots of ferromagnetic materials in the live site. The magnetic responses overlap each other during multi-target aerial survey due to the limit of flight height, which degrades largely the signal-noise rate (SNR). The GPR is also an important tool for UXO detection based on the dielectric contrast variations between media [8], but it is costly, vulnerable to the site situation and limited by the penetration depth.

Both ferromagnetic and metal targets can be detected by the electromagnetic method owing to its wide frequency band, strong penetration and high precision. Therefore, most of the geophysicists working for UXO detection prefer the electromagnetic method since most of UXO targets have metal shells. The transient electromagnetic method (TEM) is also called time-domain electromagnetic method. It is widely

used for the medium-deep resource exploration, geology prospecting and shallow engineering applications [9], [10]. In these years, the method is breaking through the shallow blind-zone of 10m and extended to detect the ultra-shallow targets such as municipal pipelines, ground grids and UXO with the rapid advances of fast-cutoff semiconductor devices, high-speed data acquisition and signal processing technology.

To find the UXO targets accurately and rapidly, one task is to develop advanced instruments for UXO survey, on the other hand, fast and reliable data processing methods are proposed by many researchers. According to the “smoke ring” effect, a typical non-linear equation is solved to obtain the target apparent resistivity and depth, and the layered geological model is built to carry out the forward and inverse analysis [11]–[13]. Based on Yee grids, the finite-difference frequency-domain (FDFD) method is proposed to avoid calculation of large linear equations [14]. However, it is very difficult to achieve the accurate resistivities and depths of the shallow and small targets by solving the nonlinear equation and inverse computation.

A magnetic dipole model of single UXO is built to solve the transient electromagnetic response by forward analysis [15], [16]. A 3-D imaging method for buried targets is proposed [17]. The underground space is first divided into many discrete grids by the finite element method (FEM). The dipole of each grid contributes to the total response, which is then compared with the actual data observed. The contribution rates are modified until the computed results match the observed data. The 3-D imaging of underground small targets can be realized but becomes more difficult for multi-target detection in the complex soil environment because only simplified soil background and single target is considered with the method. In [18], based on the transient electromagnetic method, the secondary magnetic field is directly used to draw the topology diagram and find the defaults of the power ground grid. However, Different from the eddy effect of shell-type UXO, the secondary response to the ground grid contains not only the eddy effect of underground flat steel but also the mutual inductance effect between the transmitter-receiver coils and ground grid.

The inversion results for UXO targets, especially for multiple dense UXO targets, are usually unreliable because they are of small size, no-prior distribution and located in the shallow subsurface. In this article, we abandon the troublesome nonlinear equation solution and inversion analysis [11] but acquire directly the secondary voltage with the receiver coils to draw a voltage map, which reflects really the comprehensive influences from subsurface conductivity and anomaly distribution. As a result, our work is focused on voltage image processing rather than conducting the inversion from the secondary voltage to the object resistivity.

At first, several major influences on the secondary voltage image are discussed during UXO survey, including emitting coil size, target attitude, basin effect and shell thickness, which are useful for the TEM system configuration and voltage image recognition. Furthermore, an improved watershed

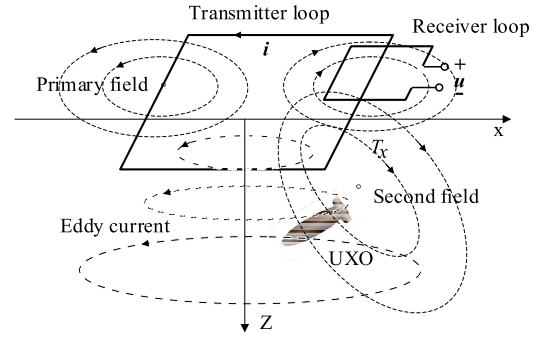


FIGURE 1. TEM survey principle.

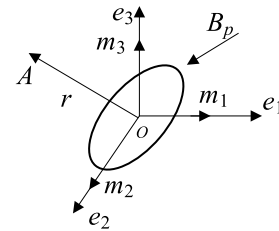


FIGURE 2. 3-D inductive dipole of finite conductor.

imaging algorithm is proposed to automatically realize the multi-target discrimination. The algorithm has been verified using simulation data and experiment data of UXO-like targets.

II. TEM SURVEY PRINCIPLE

Transient electromagnetic method is widely used for resource exploration and engineering geology in geophysical prospecting. Based on the theory of “smoke ring” effect [19] as shown in Fig.1, during transient electromagnetic prospecting the transmitter coil produces the primary magnetic field on the ground and the resultant eddy current in the subsurface generates a second magnetic field, which induces the voltage between the terminals of the receiver coil according to the electromagnetic philosophy. The UXO targets or other anomalies can be found based on the resistivity differences between the targets and the surrounding materials.

The transient electromagnetic response from a UXO target is similar to that from a finite conductor in the shallow subsurface. And the finite conductor is then equivalent to the combination of many 3-D inductive dipoles as Fig.2. The total dipole moment is represented as \vec{m} under the excitation of the primary magnetic field B_p , and the resultant secondary field B_s at point A in a solution space is:

$$\vec{B}_s = \frac{\mu_0}{4\pi} \frac{1}{r^3} [3(\vec{m} \cdot \vec{e}_r) \vec{e}_r - \vec{m}], \quad (1)$$

where \vec{e}_r is the direction vector and r is the distance from point A to the origin, and μ_0 denotes the vacuum permeability.

The total dipole moment can be decomposed into three orthogonal dipole components, each of which has a unit

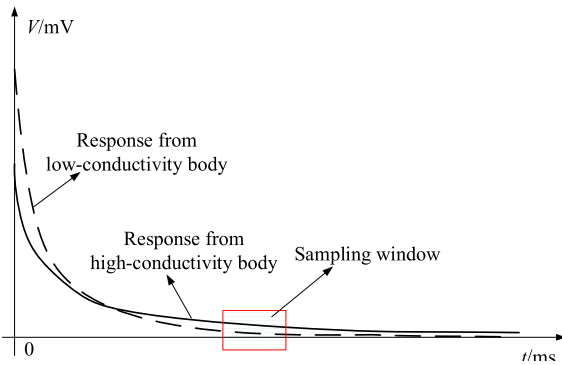


FIGURE 3. Decay law of transient electromagnetic response voltage.

vector

$$\vec{m}_i = L_i(t) (\vec{e}_i \cdot \vec{B}_p) \vec{e}_i, \quad i = 1, 2, 3, \quad (2)$$

where \vec{e}_i is unit vector of the inductive dipole \vec{m}_i , $L_i(t)$ represents the time decay feature of three dipole components, which depends on the conductivity, permeability and shape of a target. $L_i(t)$ is usually a natural exponential function. The secondary voltage decays differently when the underground targets have different conductivities and shapes. The secondary voltage is then expressed as following for the receiving coil parallel to the plane constructed by the unit vectors \vec{e}_1 and \vec{e}_2 ,

$$\begin{aligned} V &= - \int_s \frac{\partial \vec{B}_s}{\partial t} \cdot d\vec{S} \\ &= - \int_s \frac{\mu_0}{4\pi r^3} \left[3 \left((\vec{e}_3 \cdot \vec{B}_p) \frac{dL_3(t)}{dt} \vec{e}_3 \cdot \vec{e}_r \right) \vec{e}_r \cdot \vec{e}_3 \right. \\ &\quad \left. - (\vec{e}_3 \cdot \vec{B}_p) \frac{dL_3(t)}{dt} \right] d\vec{S} \end{aligned} \quad (3)$$

The secondary voltages with different initial amplitudes and decaying rates are acquired in the receiving coil for the underground medium with different resistivities, which are then used to differentiate one target from the surrounding materials.

Most of UXO targets have a metal shell. The resistivity of a metal shell is much smaller than that of the surrounding soil and rock. So the decaying rate of response voltage from UXO is also much slower than the latter according to Fig.3. The measured characteristic responses show a power-law decay function at an early time but an exponential decay function at the later time [15]. The response depends mainly on the UXO when the response from the soil and rock becomes very small. Therefore, the shape and distribution of UXO targets can be obtained according to the secondary voltage sampled within a later time window. Owing to the fast turn-off of pulse current, the time window for sampling of effective secondary voltage can be advanced so that more information of shallow objects will be obtained [20].

It is found that UXO detection by small loop TEM method is effective compared to magnetic method. Moreover, the

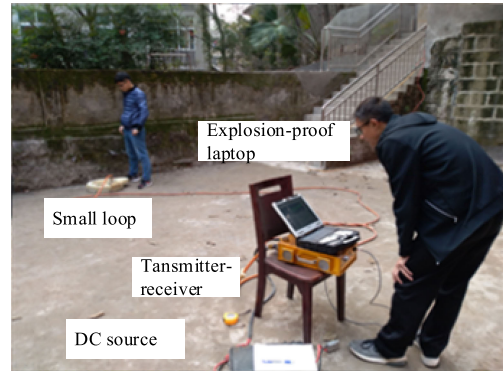


FIGURE 4. Test field of small-loop TEM system.

small loop TEM method could narrow the range of UXO location [9], [21]. Based on the transient electromagnetic method, our team has developed a small-loop shallow prospecting system, as seen in Fig.4, with high emitting moment and short turn-off time using our patented constant-voltage clamping turn-off technique. The shallow prospecting system is specific for shallow detection of UXO, pipelines, and etc.

III. MAJOR INFLUENCES ON TRANSIENT ELECTROMAGNETIC VOLTAGE IMAGE

The UXO targets are small and shallow. As a result, the induced voltages are easily influenced by the state of UXO and TEM system configuration during UXO survey. Here four major factors, including loop size, target attitude, basin effect and UXO shell thickness, are analyzed and simulated, which are helpful to recognize the transient electromagnetic voltage image.

A. LOOP SIZE

The probing depth with the transient electromagnetic method is mainly decided by the measurable time window of secondary voltage, which is majorly influenced by the apparent resistivity of probing zone and detector capability. In terms of the probing depth, a small-loop device is comparable with the large-loop one by enlarging the emitting current of transmitting coil and the equivalent area of the transmitter-receiver coils. During the shallow survey, the response from multi-turn small-loop system is proportional to the sizes and numbers of anomalies and inversely proportional to the burial depth. However, it is difficult to distinguish two anomalies if their distance is smaller than the side length or diameter of the coils. A small-loop transient electromagnetic system, as shown in Fig.4, has been developed by our team to detect the ultra-shallow targets after optimizing the size and structure of coils.

The secondary voltage maps are separately drawn in the left panel and right panel of Fig.5 when using a 0.9m-diameter loop and a 0.4m-diameter one. As can be seen, two small targets are separately circled in case of a smaller loop system.

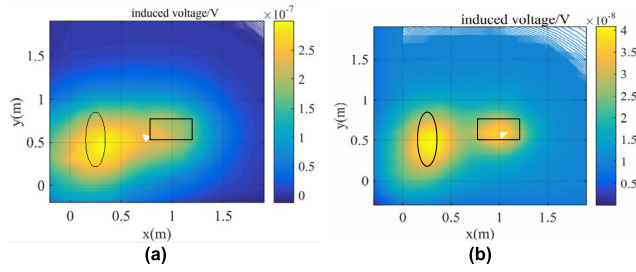


FIGURE 5. Influence of loop size on the target resolution. (a) 0.9m-diameter coil. (b) 0.4m-diameter coil.

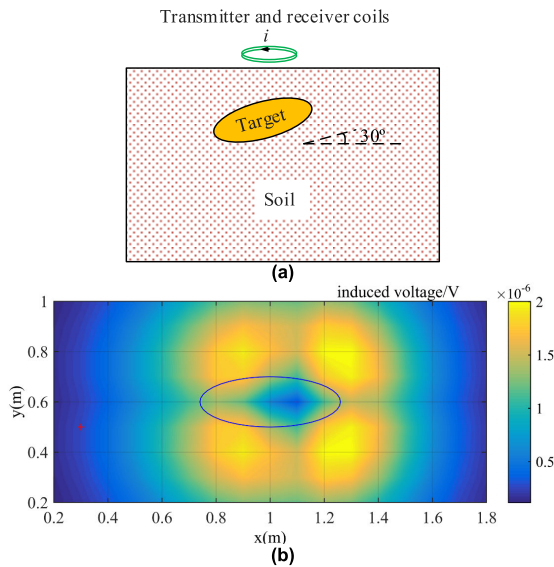


FIGURE 6. Influence of target attitude on the secondary voltage. (a) Target model. (b) Secondary voltage map.

B. TARGET ATTITUDE

If the burial depth of a finite-size underground target is much bigger than its diameter, the magnetic field on the ground from a finite-size underground target is similar to that from a ball-like target. However, clearer recognition of underground targets is achievable owing to the shorter cut-off time, optimized coil configuration and versatile signal processing methods. Most UXO targets have a long ellipsoidal shell, and seldom lie in the subsurface flat or vertically but with an incline angle to the horizontal plane. It is helpful to remove the UXO target and differentiate the metal scraps by knowing the attitude and shape of the UXO target.

A high-conductivity ellipsoidal body is laid at an incline angle of 30 degrees as in Fig.6 (a). The response is asymmetric along the long axis of the ellipsoidal body. Accordingly, it can be judged that the target is not a ball-like target and reclines underground in the way that the left end is lower than the right end.

C. BASIN EFFECT OF ULTRA-SHALLOW DETECTION

When the target is very shallow, a strong secondary eddy current is created underground near the primary coil ring, which

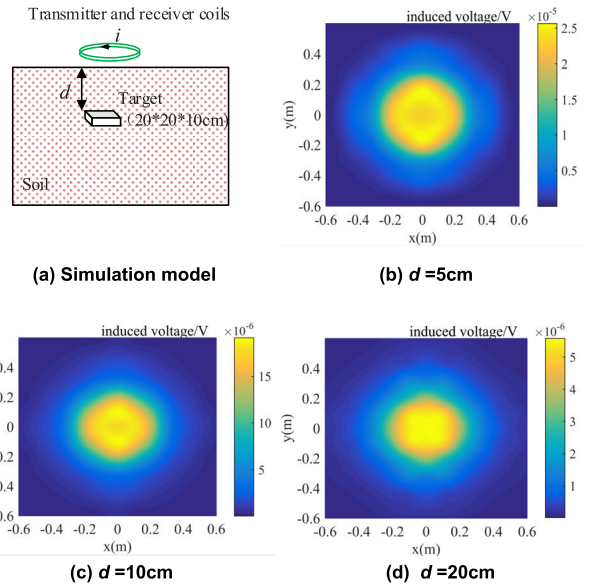


FIGURE 7. Basin effect during shallow detection.

makes the secondary response above the target weaker than that surrounding it. This is the basin effect during small-loop detection.

As shown in Fig.7 (a), a rectangular metal target (20*20*10cm) is buried in the shallow soil layer and the transmitter coil and receiver coil are respectively used to emit the primary magnetic field and acquire the secondary voltage during power-off. As shown in Fig.7 (b)-(d), the basin effect is obvious when the target is 5cm deep and will disappear with the burial depth increasing. And also, the basin effect exists in a different depth range considering the different coil diameters and the size and conductivity of a target.

D. SHELL THICKNESS OF UXO

Among the shallow metal targets, the UXO usually has a shell structure, which is different from the power ground grid, the block-like metal targets and the metal scraps. According to the transient electromagnetic method, the eddy current is established inside the underground UXO target under the primary magnetic field excited by the transmitting current. The resistance along eddy ring within the metal shell is too large in case of very thin shell. As a result, the eddy current is small and the secondary magnetic field is very weak. On the contrary, higher secondary voltage can be acquired when the resistance of eddy ring become smaller with the shell thickness increasing. However, this is not always the case. The eddy current decays slowly and the secondary response drops down instead when the UXO shell continues to become thick as seen in Fig.8.

Therefore, the response from a metal shell is much stronger than that from solid metal body. It is also proved through finite-element simulation there exists a shell thickness for the strongest response. According to the relation between the shell thickness and response strength, it is useful to judge

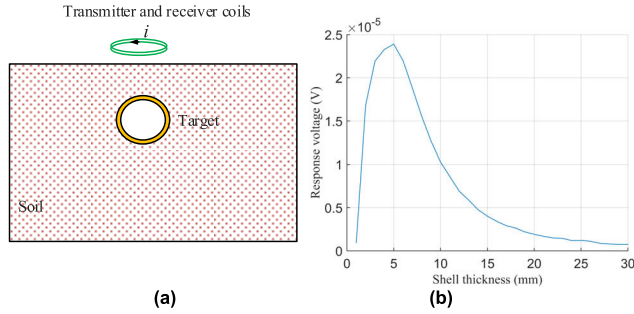


FIGURE 8. Influence of shell thickness on the secondary voltage. (a) Target model. (b) Secondary voltage changes with shell thickness.

the UXO type, shell thickness, erosion degree and the false targets.

IV. IMAGING ALGORITHM FOR DENSE TARGETS

A. ALGORITHM PRINCIPLE

Morphological method is widely utilized in object identification and remote sensing image classification [22], [23]. Watershed transform is originally developed in the field of topography, and it is found to be useful in digital image processing. According to the geomorphology theories, the gray value of each pixel in a picture is corresponding to a sea level, and the local minimum and its ambient zone are integrally called as a catchment basin. The boundary of a catchment basin is used as the watershed lines. Watershed transform has been widely applied in image segmentation algorithms to separate an image into many homogeneous non-overlapped closed regions.

However, over-segmentation of an image exists generally because the traditional watershed algorithm is sensitive to the noise. On the other hand, under-segmentation appears typically resulting from secondary voltage overlapping during transient electromagnetic imaging of dense targets. So the marker of minimum is introduced to reduce the over-segmentation in this article. And also an improved marking method is proposed to prevent under-segmentation so that an image of induced voltages is segmented effectively into some non-overlapped closed regions, each of which represents a possible UXO target.

The algorithm principle is demonstrated in Fig.9. At first, a 3-D induced voltage map is transformed into a gray-level image within which large voltages exist in the zones of large gray values and low voltages does in the zones of small gray values. The burrs and noises in a gray-level image can be then erased by erosion and reconstruction to prevent the over-segmentation resulting from pseudo-peak. The maximums will form one or more closed zone after erosion of peak zones in the secondary voltage map.

1) BACKGROUND MARKING

The zones with low induced voltages and far from the targets in a gray-level image are delimited by background marking. At first a binary-value image is obtained after the

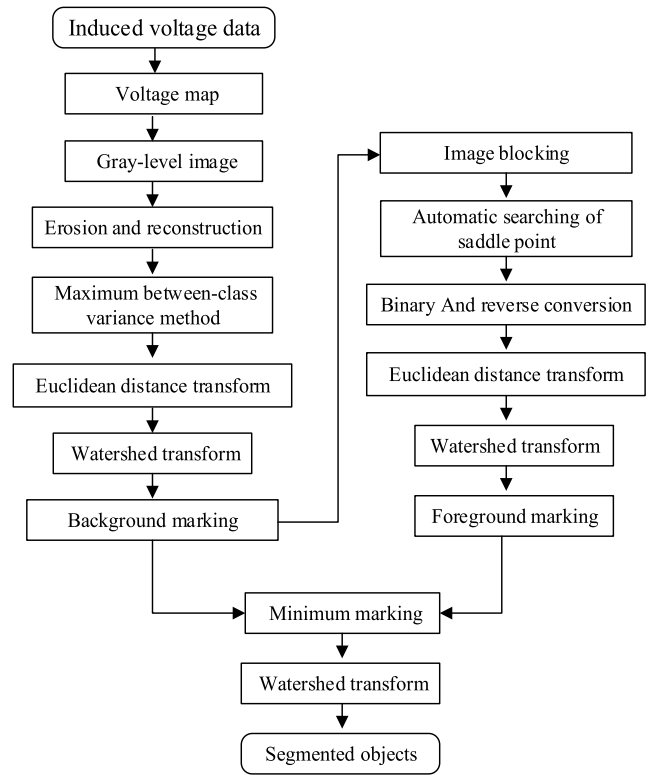


FIGURE 9. Imaging algorithm of dense targets.

binary-conversion of reconstructed image based on the maximum between-class variance method as in Appendix A. And then the typical watershed algorithm is employed to obtain the background markers followed by the Euclidean distance transform.

The maximum between-class variance method is a typical threshold segmentation method. The best threshold for image segmentation can be achieved when the class variance between the target and background is largest.

The between-class variance for the best threshold k^* is

$$\sigma_B^2(k^*) = \max_{1 \leq k < L} \sigma_B^2(k), \quad (4)$$

where the between-class variance $\sigma_B^2(k)$ is calculated as Appendix A.

The distance between each pixel point and the nearest background point can be solved through the following distance transform,

$$[D(f)](p) = \min\{d(p, q) | f(q) = 0\}, \quad (5)$$

where the distance function d denotes Euclidean distance,

$$d((x_1, y_1), (x_2, y_2)) = \sqrt{(x_2 - x_1)^2 + (y_2 - y_1)^2}. \quad (6)$$

2) FOREGROUND MARKING

The target position can be detected according to the gray-level image of the induced voltage. A threshold is selected to mark the induced voltage distribution of the target so that

the watershed lines after threshold marking encircle the distribution region of a target. The transient electromagnetic induced voltages from a single target obey usually a normal distribution but the induced voltages will overlap when two targets are close to each other. As a result, several targets will be possibly regarded as one target if the threshold is too small, that is, the under-segmentation will appear during transient electromagnetic imaging. For the induced voltage distribution of one survey line, the threshold should be higher than the valley value within the overlapping section between two peaks. Different from one-line survey, the saddle point located within the overlapping region is used as the segmentation threshold for the multi-line voltage distribution. Therefore, the true saddle point is first found to separate two or more targets in case of serious overlapping.

A higher threshold is selected to separate all the targets when there are several targets with overlapping induced voltage regions. Different thresholds are defined for different overlapping situations, so blocking of the gray-level image is necessary. The watershed lines from the background marking are used to cut the gray-level image apart into several regions except that those targets with serious induced voltage overlapping. There is at least a target within each of segmented blocks. The threshold is decided by the maximum between-class variance method of the whole image when there is only a target or several targets with less obvious overlapping. On the other hand, it is key to find the saddle point for the threshold in case of dense targets to be detected and serious overlapping of induced voltage distribution. An algorithmic framework of generalized primal-dual hybrid gradient methods is provided for saddle point problems, but strict constraints are needed for the convergence of algorithm [24]. In our work, an adaptive saddle-point search (ASS) method is proposed based on the simple geometry operations. The algorithm flowchart is illustrated as Fig. 10 and the key steps are followed to remove the pseudo saddle point and prevent under-segmentation.

Step 1: find the maximums from the gray-level image after erosion and reconstruction. Each geometry center of the small connected regions corresponds to a maximum.

Step 2: draw lines on the x-y plane by connecting the projection points of every two geometry centers (such as A and B in Fig.11) and find the smallest induced voltage (such as C) along each line.

Step 3: move the line between the two projection points along the horizontal axis or vertical axis of the reference coordinate system. The corresponding curve between two geometry centers doesn't necessarily pass the saddle point because the overlapping secondary voltages from dense targets lead to the saddle distortion, that is, the minimum point may be a pseudo saddle point (such as C). A new minimum of induced voltage is found every move of a pixel.

Step 4: find the biggest one from all the minimums, which is then used as the saddle point (such as point S) between two peaks.

A saddle point is found between every two peaks within a block. The gray value at the saddle point is selected as the

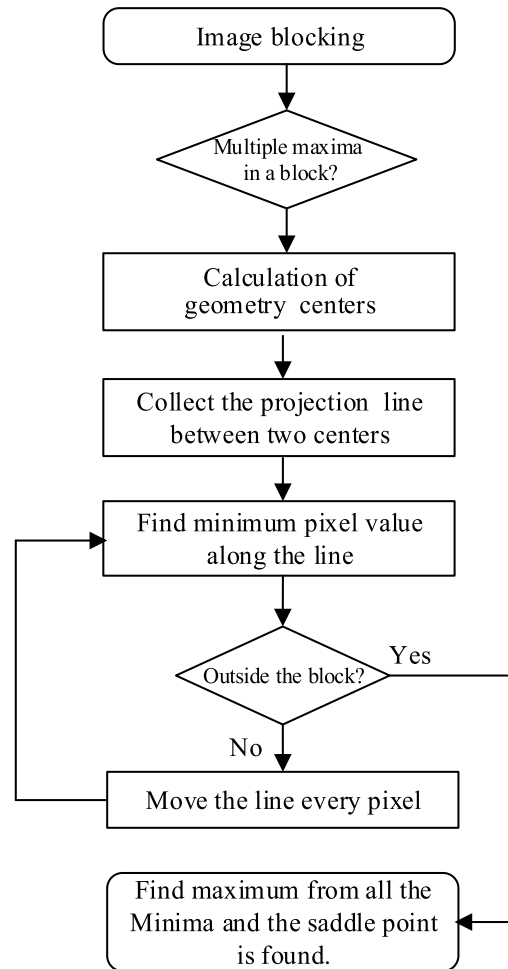


FIGURE 10. ASS method (adaptive saddle-point search method).

threshold of a block so as to separate all the targets in the block.

After binary conversion based on the threshold obtained as above, each block image is inverted so that the peak value of induced voltage is changed to a valley value. Then the distance transform and watershed transform are successively carried out and the results are used as the foreground marker. The overlapping response voltages are automatically separated owing to the foreground marker so that every target has a separate distribution region.

The minimum marking of an original image is performed following the foreground marking and background marking, according to the mathematical morphology theory,

$$I^{WS} = \text{IMMIN}(I|I^{fmark}|I^{bmark}), \quad (7)$$

where $\text{IMMIN}(\bullet)$ denotes the minimum marking operation according to the mathematical morphology theory.

Finally, the marked image evolves into a picture of target distribution through watershed transform and each small connected region represents the domain of a target.

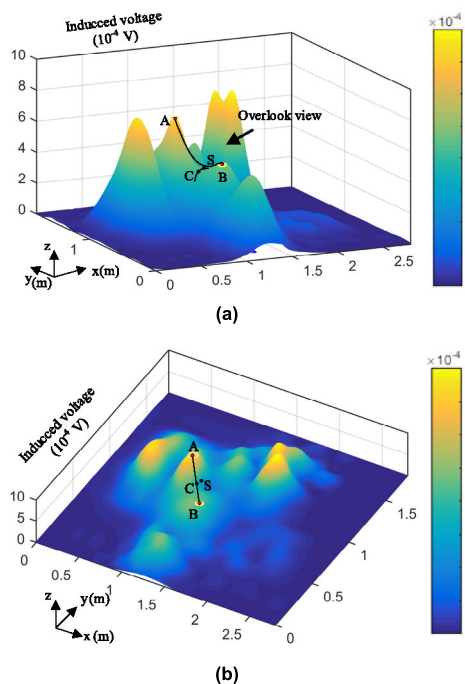


FIGURE 11. Adaptive search of saddle point. (a) Secondary voltage map. (b) Overlook view of (a).

B. VERIFICATION OF IMAGING ALGORITHM

To verify the shallow survey of UXO targets by the transient electromagnetic method and the algorithm of multi-target identification, a five-target transient electromagnetic model is built and simulated through a finite-element software. Five metal targets at a depth of 0.5m are used to simulate five shallow UXO targets, including three balls, an ellipsoid and a cuboid. The metal targets have very high conductivity and the soil has high resistivity of 1Ω.m. A multi-turn coil is used as the transmitting coil, within which the exciting current is created at high level and the secondary response is acquired during power off. Based on our electromagnetic system in use, a 30-ampere pulsed current with a short cut-off time of 20 microseconds flows through a small coil with a diameter of 0.5m.

The five metal targets are placed as Fig.12 (a). According to the transient electromagnetic method, the decay rate of the secondary voltage from a conductive metal target is much smaller than that from the soil medium at later time as Fig.3. Therefore, the later-time voltages are acquired to highlight the response resulting from the metal targets. The inductive voltages are depicted in Fig.12 (a) according to the simulation data. The response contours from three small balls are weak but they hardly overlap when the balls are located far from each other. So three ball-type targets are easily separated.

However, it is difficult to separate the ellipsoid and cuboid targets due to the overlapping contour plots when they are close to each other even if they induce larger responses. Fortunately, according to the algorithm proposed in the paper the whole map is partitioned into 4 blocks as Fig.12 (b) after

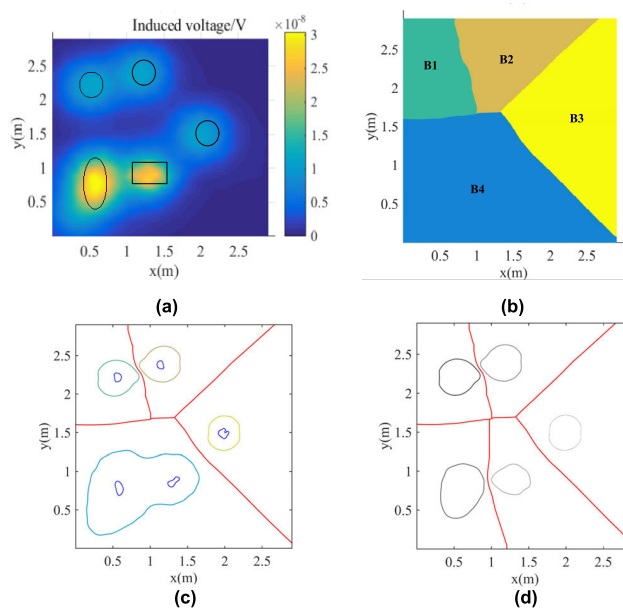


FIGURE 12. Image Segmentation of multiple targets. (a) Induced voltage map. (b) Image blocking. (c) Over-segmentation and under-segmentation. (d) Target segmentation by ASS method.



FIGURE 13. Test field of UXO-like targets.

background marking and further the two overlapping targets are separated in B4 as Fig.12 (d) using improved foreground marking. If the threshold for segmentation is too big, the very small closed regions as seen in Fig. 12 (c) cannot represent the real objects due to the over-segmentation. On the other hand, if the threshold is too small, the neighboring targets in the segmented image tend to join together as seen in B4 block of Fig.12 (c) as a result of the under-segmentation. Accordingly, the five objects are well identified by the ASS method as seen in Fig.12 (d), which successfully avoids over-segmentation and under-segmentation.

V. APPLICATION OF IMAGING ALGORITHM TO FIELD TEST DATA

A field test is carried out to verify the effectivity of the electromagnetic system and the imaging method on UXO-like targets. Three UXO-like targets are buried subsurface as Fig.13. Target ① is 30*15*5cm in size and 0.3m in depth. Target ② is 30*15*3cm in size and one end is 0.3m in depth but the opposite end declines. Target ③ is 30*15*5cm in size and 0.4m in depth. A small-loop system is used for the test.

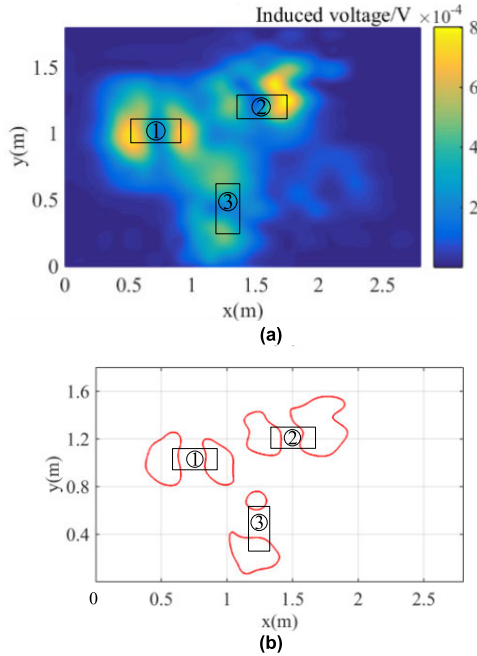


FIGURE 14. UXO-like target detection from test data. (a) Secondary voltage map. (b) Target segmentation.

According to the induced voltage acquired by the transient electromagnetic system, the contour map is demonstrated as Fig.14 (a). The map is not very regular near the targets under test because sparse survey points are defined for the survey efficiency when the loop is moved every 10cm. In addition, the response encircling a target is stronger than that on top of the target due to the basin effect when using smaller loop system to detect ultra-shallow targets. There exists serious voltage overlapping between target ① and ③.

As seen in the low panel of Fig.14, three pairs of connected domains are formed with the improved morphology algorithm, each of which represents a target considering the basin effect. In addition, the position and attitude of each target can be still distinguishable. Target ① has a pair of big connected domains while target ③ has a pair of small connected domains because of the difference of buried depth. The inclined attitude of target ② is illustrated through very different connected domains at two ends.

VI. CONCLUSION

The transient electromagnetic method is feasible for shallow UXO survey. A small-loop TEM system is necessary to enhance the resolution of dense target identification. The basin effect appears during detection of ultra-shallow targets with a small-loop system but it disappears with buried depth increasing. The secondary response becomes stronger than that from a block-like body since most UXO targets have shell structures. And also there exists a best thickness for strongest induced voltage, which is useful to judge the UXO types, shell thickness, erosion degree and the false targets.

Complex inversion of apparent resistivity is avoided by direct imaging of transient electromagnetic data based on the mathematical morphology. The over-segmentation and under-segmentation of voltage image can be reduced by adaptive search of the optimal threshold when combining foreground marking with background marking. The imaging algorithm in the work is also proved effect in case of dense buried targets and sparse sampling data.

APPENDIX A

If the pixels of a picture are expressed as L gray levels, then the total number of pixels $N = n_1 + n_2 + \dots + n_L$, where the subscripts represent the gray levels. For convenience, a normalized gray-level histogram is regarded as the probability distribution of the image,

$$p(i) = n_i/N \dots p(i) \geq 0, \sum_{i=1}^L p(i) = 1. \tag{8}$$

The pixel points are divided into two classes according to the gray-level threshold k , of which class C_1 represents the background and class C_2 represents the targets. The probabilities of class occurrence are expressed as following,

$$q_1(k) = \sum_{i=1}^k p(i) \dots q_2(k) = \sum_{i=k+1}^L p(i) \tag{9}$$

The class mean levels are defined as,

$$\mu_1(k) = \sum_{i=1}^k \frac{i \cdot p(i)}{q_1(k)} \dots \mu_2(k) = \sum_{i=k+1}^L \frac{i \cdot p(i)}{q_2(k)} \tag{10}$$

And the class variances are,

$$\begin{aligned} \sigma_1^2(k) &= \sum_{i=1}^k [i - \mu_1(k)]^2 \frac{p(i)}{q_1(k)} \dots \sigma_2^2(k) \\ &= \sum_{i=k+1}^L [i - \mu_2(k)]^2 \frac{p(i)}{q_2(k)}. \end{aligned} \tag{11}$$

The between-class variance is expressed as

$$\sigma_B^2(k) = q_1(k) \cdot q_2(k) \cdot [\mu_1(k) - \mu_2(k)]^2. \tag{12}$$

REFERENCES

- [1] P. B. Weichman, "Validation of advanced EM models for UXO discrimination," *IEEE Trans. Geosci. Remote Sens.*, vol. 51, no. 7, pp. 3954–3967, Jul. 2013.
- [2] V. Paoletti, A. Buggi, and R. Pašteka, "UXO detection by multiscale potential field methods," *Pure Appl. Geophysics*, vol. 176, no. 10, pp. 4363–4381, Oct. 2019.
- [3] Y. Li, S. G. R. Devriese, R. A. Krahenbuhl, and K. Davis, "Enhancement of magnetic data by stable downward continuation for UXO application," *IEEE Trans. Geosci. Remote Sens.*, vol. 51, no. 6, pp. 3605–3614, Jun. 2013.
- [4] M. P. Bray and C. A. Link, "Learning machine identification of ferromagnetic UXO using magnetometry," *IEEE J. Sel. Topics Appl. Earth Observ. Remote Sens.*, vol. 8, no. 2, pp. 835–844, Feb. 2015.
- [5] M. Combrinck, "Transient electromagnetic exploration techniques: Can they be applied to the landmine discrimination problem?" *J. Afr. Earth Sci.*, vol. 33, nos. 3–4, pp. 693–698, Jan. 2001.

- [6] L.-P. Song, D. W. Oldenburg, L. R. Pasion, S. D. Billings, and L. Beran, "Temporal orthogonal projection inversion for EMI sensing of UXO," *IEEE Trans. Geosci. Remote Sens.*, vol. 53, no. 2, pp. 1061–1072, Feb. 2015.
- [7] J. S. Kobashigawa, H.-S. Youn, M. F. Iskander, and Z. Yun, "Classification of buried targets using ground penetrating radar: Comparison between genetic programming and neural networks," *IEEE Antennas Wireless Propag. Lett.*, vol. 10, pp. 971–974, 2011.
- [8] X. Núñez-Nieto, M. Solla, P. Gómez-Pérez, and H. Lorenzo, "Signal-to-noise ratio dependence on ground penetrating radar antenna frequency in the field of landmine and UXO detection," *Measurement*, vol. 73, pp. 24–32, Sep. 2015.
- [9] C. Yu, Z. Fu, H. Zhang, H.-M. Tai, and X. Zhu, "Transient process and optimal design of receiver coil for small-loop transient electromagnetics," *Geophys. Prospecting*, vol. 62, no. 2, pp. 377–384, Mar. 2014.
- [10] Z. Jiang, S. Liu, and R. Malekian, "Analysis of a whole-space transient electromagnetic field in 2.5-dimensional FDTD geoelectric modeling," *IEEE Access*, vol. 5, pp. 18707–18714, 2017.
- [11] S. Qin, Y. Wang, H.-M. Tai, H. Wang, X. Liao, and Z. Fu, "TEM apparent resistivity imaging for grounding grid detection using artificial neural network," *IET Gener., Transmiss. Distrib.*, vol. 13, no. 17, pp. 3932–3940, Sep. 2019.
- [12] S. Qin, Y. Wang, Z. Xu, X. Liao, L. Liu, and Z. Fu, "Fast resistivity imaging of transient electromagnetic using ANN," *IEEE Geosci. Remote Sens. Lett.*, vol. 16, no. 9, pp. 1373–1377, Sep. 2019.
- [13] Q. Meng, X. Hu, H. Pan, and Y. Xi, "Apparent resistivity for transient electromagnetic induction logging and its correction in radial layer identification," *J. Appl. Geophys.*, vol. 151, pp. 328–342, Apr. 2018.
- [14] H. Luan, Y. Geng, Y. Yu, and S. Guan, "Three-dimensional transient electromagnetic numerical simulation using FDFD based on octree grids," *IEEE Access*, vol. 7, pp. 161052–161063, 2019.
- [15] S. Chen, S. Zhang, J. Zhu, and X. Luan, "Accurate measurement of characteristic response for unexploded ordnance with transient electromagnetic system," *IEEE Trans. Instrum. Meas.*, vol. 69, no. 4, pp. 1728–1736, Apr. 2020.
- [16] L. R. Pasion and D. W. Oldenburg, "A discrimination algorithm for UXO using time domain electromagnetics," *J. Environ. Eng. Geophys.*, vol. 6, no. 2, pp. 91–102, Jun. 2001.
- [17] W. Xie, X. Zhang, and Y. Mu, "A novel 3-D imaging method for subsurface targets based on time-domain electromagnetic induction system," *IEEE Geosci. Remote Sens. Lett.*, vol. 17, no. 6, pp. 938–942, Jun. 2020.
- [18] C. Yu, Z. Fu, G. Wu, L. Zhou, X. Zhu, and M. Bao, "Configuration detection of substation grounding grid using transient electromagnetic method," *IEEE Trans. Ind. Electron.*, vol. 64, no. 8, pp. 6475–6483, Aug. 2017.
- [19] Z. R. Dennis and J. P. Cull, "Transient electromagnetic surveys for the measurement of near-surface electrical anisotropy," *J. Appl. Geophys.*, vol. 76, pp. 64–73, Jan. 2012.
- [20] X. Zhu, X. Su, H.-M. Tai, Z. Fu, and C. Yu, "Bipolar steep pulse current source for highly inductive load," *IEEE Trans. Power Electron.*, vol. 31, no. 9, pp. 6169–6175, Sep. 2016.
- [21] S. Kukita and H. Mizunaga, "UXO detection using small loop TEM method," in *Proc. 11th SEGJ Int. Symp.*, Yokohama, Japan, Nov. 2013, pp. 94–97.
- [22] X. Xu, J. Li, X. Huang, M. Dalla Mura, and A. Plaza, "Multiple morphological component analysis based decomposition for remote sensing image classification," *IEEE Trans. Geosci. Remote Sens.*, vol. 54, no. 5, pp. 3083–3102, May 2016.
- [23] T. Lei, X. Jia, T. Liu, S. Liu, H. Meng, and A. K. Nandi, "Adaptive morphological reconstruction for seeded image segmentation," *IEEE Trans. Image Process.*, vol. 28, no. 11, pp. 5510–5523, Nov. 2019.
- [24] B. He, F. Ma, and X. Yuan, "An algorithmic framework of generalized primal–dual hybrid gradient methods for saddle point problems," *J. Math. Imag. Vis.*, vol. 58, no. 2, pp. 279–293, Jun. 2017.



XUEGUI ZHU received the B.S. and M.S. degrees in mechanical engineering from Southwest Petroleum University, Sichuan, China, and the Ph.D. degree in electrical engineering from Beijing Jiaotong University, Beijing, China. Since 2008, he has been working at Chongqing University and the Science and Technology on Near-Surface Detection Laboratory, where he is currently engaged in nondestructive testing and geophysical prospecting.



YU SHU received the B.S. degree in electrical engineering from Chongqing University, Chongqing, China, where he is currently pursuing the M.S. degree in electrical engineering.

His research interests include image processing and embedded system development.



CHAOPENG LUO is currently pursuing the master's degree in electrical engineering with the National University of Defense Technology.

He is an Engineer with the Science and Technology on Near-Surface Detection Laboratory, China. His research interest includes unexploded ordnance detecting.



FUSHUO HUO received the B.S. degree in electrical engineering from the China University of Mining and Technology, Xuzhou, China. He is currently pursuing the M.S. degree in electrical engineering with Chongqing University, China.

His research interests include image processing and intelligent information processing.



WANG ZHU is currently pursuing the master's degree in communications engineering with the School of Microelectronics and Communication Engineering, Chongqing University, China.

His research interests include signal processing and wireless power transfer.

• • •